25th ABCM International Congress of Mechanical Engineering
October 20-25, 2019, Uberlândia, MG, Brazil

ON THE INVESTIGATION OF ORDINARY SPRAY NOZZLE IMAGES TO DETECT ITS HEALTH CONDITION VIA IMAGE SIGNAL PROCESSING

Gabriel Alves Costa
Fabrício César Lobato de Almeida
Marcos Silveira
Paulo José Paupitz Gonçalves
São Paulo State University - UNESP, Av. Eng. Luiz Edmundo Carrijo Coube, 14-01, Vargem Limpa, Bauru - SP
gabriel.a.costa@unesp.br, fabricio.lobato@unesp.br, marcos.silveira@unesp.br, paulo.paupitz@unesp.br

Abstract. *Spray nozzles are commonly used in crops irrigation, selected according to the desired spray distribution. The wear present in nozzles results in failures in spray distribution, compromising the uniformity of application. This work intends to estimate the health condition of hollow cone nozzles. Hence, image of sprays can be used to estimate the nozzle health condition, which is directly related to wear level. Four ordinary side view images of spray nozzles are taken, using a test bench developed by the company Spraying System Co. The pre-processing consists in getting a spray cross-section intensity vector near to the nozzle discharge, which is then filtered to attenuate the effects of undesirable noise and enhanced by applying the power-law transformation method. This gives how the intensity signals changes along the pixels (spatial domain). To estimate the health condition of the nozzles, four methods were proposed: the area under intensity curves, the Fourier series coefficients of signals, the auto-correlation of each signal and the cross-correlation of each position signal to the mean signal. The methods were effective to present differences that can estimate the quality of a nozzle, explaining the faults in uniformity for the cases of defective nozzles, comparing to a good one.*

Keywords: *nozzle wear, image processing, health condition, power-law transformation*

1. INTRODUCTION

Spray nozzles are devices used to split liquid jets into liquid drops according to the desired spray characteristics. There are many types of nozzles available from high resistance applications, such as abrasive waterjet machining, to general applications, like irrigation. However, its lifespan is dependent upon the wear level, which changes the spray pattern and leading to a reduction of its effectiveness resulting in a waste of fluid. According to Barber (2009), it is estimated that about U$180,000.00 can be over spent as extra cost due to wear (15% increase in orifice area by wear) in spray nozzles each year per machine. Hence, ways of predicting the wear level in spray nozzles have been under constant development to estimate its heath condition.

The focus of this work is on irrigation systems and water wastage caused by wear nozzles, so that studies conducted on the prediction of wear characteristics based on experimental analysis and numerical modeling will be introduced. Ozkan *et al.* (1992) used a mixture of water and abrasive (particles) to simulate the wear on nozzles, analyzing experimentally the variation in the flow rate and in the uniformity of the spray due to the level of wear. Using a test rig with V shape channels to observe the flow rate in different regions of the spray, the authors noted little difference in spray width, but a significant change in flow in central region of spray, explaining failure in the uniformity. Kecskésné Nagy *et al.* (2014), using the experimental proceedings of Ozkan *et al.* (1992) to simulate the wear, analyzed the quality of the spray based on the characteristics of distribution and size of the droplets using a surface of sensitive paper, observing a scattering increment due to wear. Krishnaswamy and Krishnan (2002) used a database of spray characteristics together with different flow rates to develop a regression model used as an input for training neural network algorithms to predict nozzle health condition (wear level). Xu and Yan (2016) developed an algorithm for numerical analysis of wear nozzles where the fluid flow behavior, the mass loss rate in the device and the deformation of boundaries walls, region which is most impacted by the presence of wear, together with the effects on the pressure and velocity.

In Brazil, however, researches in this area are mostly on spray drift. Bauer and Raetano (2004) investigated ways of reducing pulverization volume but keeping the spray distribution, by using an experimental rig to analyze the nozzle positioning, observing height, angular position and space between nozzles, optimizing the application. Maciel *et al.* (2018) used a climatic chamber with a wind tunnel together with a heating system to simulate different atmospheric conditions and to evaluate the interference of such parameters in droplets distribution and drift. Godinho Jr. *et al.* (2018) verified the reduction of droplet drift effect using anti-drift nozzles with air induction by adding chemical products to the fluid in an attempt to "control" its physical and chemical properties, resulting in a better deposition with reduction of the

drift.

The objective of this work is to investigate experimentally side-view images of sprays generated by hollow cone nozzles as an attempt to estimate its health condition, which is believed to be the first of this kind for hollow cone nozzles. This is carried out by obtaining intensity signals from the images, applying signals processing and digital image processing techniques to estimate the nozzle health condition.

2. DATA ACQUISITION AND PRE PROCESSING

Side-view images of the spray are collected in a test rig used to carry out visual assessment of spray nozzles. The company *Spraying Systems Co.* provided the test rig. This rig, presented in Fig. 1, is composed by a "closed loop" where the water recirculates throughout the system, a quick-coupling mechanism composed by a pneumatic piston and a control system where the nozzle can be rapidly attached and released and led lights responsible to enhance the spray patterns. The flow pressure was kept at 40 psi, according to the norm NBR 13769 (ABNT, 1997), which define standards to test methods for sprinkler nozzles. Moreover, the spray nozzle condition is then assessed by observing the uniformity of the spray, so that when the spray distribution does not match to the designed one, the nozzle is then disposed.

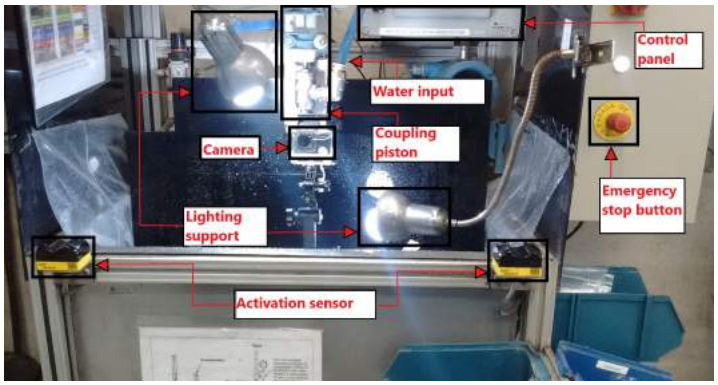

Figure 1. Flow test rig

The image collection is performed with a GoPro camera fixed on the test rig right in front of the nozzle. Furthermore, videos of 10 seconds at a rate of 60 fps and resolution 1920x1080 pixels were taken. An average of the frames is then calculated reducing the noise contained in the images. A total of 17 ceramic hollow cone nozzles were tested, being 6 in good quality and 11 with defect, among which 3 were selected and investigated. The nozzle were named as "N1", "N2" and "N3", related to nozzles in good, very bad and roughly bad conditions, respectively. The images of the front, right, back and left side views were taken. A comparison between their shapes can be used to estimate the health condition of such nozzles.

The image given by the frames are 3D ones having pixels in the "x" and "y" directions and the intensity in the "z" direction. However, the cross-section of the spray is taken instead in order to reduce the image size and enhance signal processing computational cost. Hence, the pixels along the "x" axis together with the spray intensity are taken at a certain point near by the nozzle jet, so that, the pattern of the nozzle cross-section is obtained. This signal can be used as a representative characteristic of the spray nozzle condition. Figure 2(a), (b) and (c) show the N1, N2 and N3 cases, respectively, where the position of the cross-section, which will be used for the analisys is highlighted and defined by the blue line located at 300 pixels in the "y" direction.

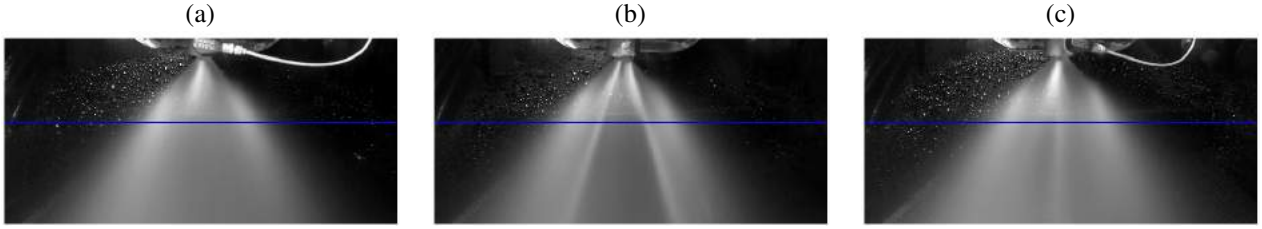

Figure 2. Spray images in position 1 for (a) N1 (b) N2 (c) N3

The cross-section "plot" is shown in Fig. 3. The blue line is the raw data (cross-section) without any pre-processing procedure, where can be observed spikes in the data. This is due to the water drops (noise) located in the wall behind the spray jet. The red line is the result of filtering, and the magenta traced-line is the power-law transformation, both explained forward.

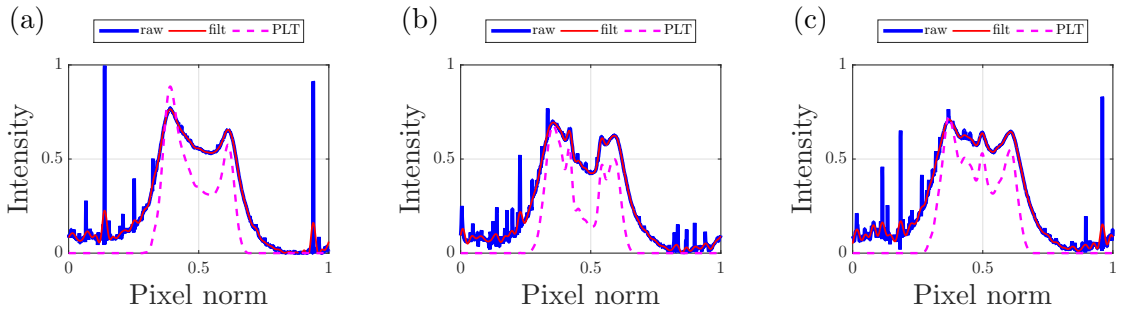

Figure 3. Comparison of a signal without processing technics, after filtering and after Power-Law transformation for (a) N1, (b) N2 and (c) N3

A pre-processing procedure is applied to reduce the effects of such noise in the raw data. For this, a low-pass Butterworth filter was used to filter the spikes effect (high frequency content), which transfer function is given by Eq. (1), adapted from Shin and Hammond (2008).

$$H(u) = \frac{1}{\sqrt{1 + [u/u_0]^{2o_d}}}, \tag{1}$$

where o_d is the filter order, set to 8, and u_0 is the half-power frequency, set at 35 cycle/pixel, which is the value that reduces the intensity due to the presence of spikes in the data but keeps the characteristics of the spray condition. The red line given in the Fig. 3 shows the effect of filtering, reducing the intensity peaks and noisy variations in signals, keeping the variations occurred because of the faults on sprays.

The contrast setting is also applied to highlight the intensity variations in the jet. This is achieved via an intensity transformation technique developed by Gonzalez *et al.* (2008) called Power-Law Transformation being the output s given by

$$s = cr^{\gamma}, \tag{2}$$

where r is the input intensity, γ is the power factor and c is the gain, which is set to 1 for the investigated problem. The power factor γ controls the behavior of transformation, so that values greater than 1 make the image darker, and values smaller than 1 make the image lighter. Together with the transformation was applied the contrast stretching technique, an intensity input range limitation making the values for r below the lower limit to be associated with $s = 0$ and above the upper limit to be associated with $s = 1$.

The limits for the contrast stretching were defined based on the values presented in the intensity signals, with lower and higher limits set at 0.2 and 0.8, respectively. Hence, values below 0.2 are considered very dark and above 0.8 very light. The power factor is set at $\gamma = 2$, as this is the value which keeps the low intensities much darker but with no change in the spray characteristics. The magenta traced-line given in the Fig. 3 shows how the cross-section "plot" is changed by applying the contrast transformation. The measure of the nozzle health condition is achieved via the cross-section plot given by the magenta line (pre-processed data), which will be investigated in the next section.

3. QUALITY MEASURES TO ASSESS THE CONDITION OF SPRAY NOZZLES

For a nozzle in good condition, the spray has a uniform distribution and has no change in its pattern independent of each view (front, right, back and left views) is taken. Hence, the intensity signals collected in the four positions are similar when the nozzle is considered in a good health condition. On other hand, nozzle subjected to wear fault can change such pattern according to the analyzed position. As a basis for comparison, a mean of the signals at the four positions was obtained for each nozzle.

Four methods were developed to estimate the health condition of the nozzles analyzed, being them: area under the intensity curves, Fourier series coefficients, auto-correlation function of each signal and cross-correlation functions of each position signal with the mean signal. These methods are presented in following subsections.

3.1 Area analysis

Figure 4(a), (b) and (c) show the mean cross-section plot (thick-black line) calculated using the side-views for the N1, N2 and N3 cases, respectively. Moreover, the side-views are also shown Fig. 4, numbered as 1, 2, 3 and 4 for front, right, back and left views respectively, and overlaid for a better visualization. The pixel axis (x axis) was normalized from 0 to 1 with respect to the maximum pixel present in the analyzed range.

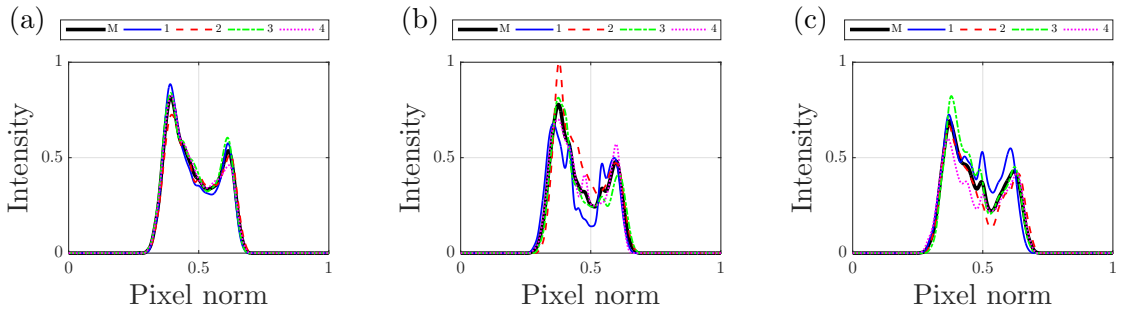

Figure 4. Intensity signal in four positions and mean signal for (a) N1, (b) N2 and (c) N3

It is observed that the cross-sections for the N1 condition is similar to the mean signal. However, this is not the case for the conditions N2 and N3. Figure 5 shows a comparison between the area calculated underneath the cross-section plot for each side-view, the area under the mean intensity vector inclusive. The N1 condition has the most uniform distribution.

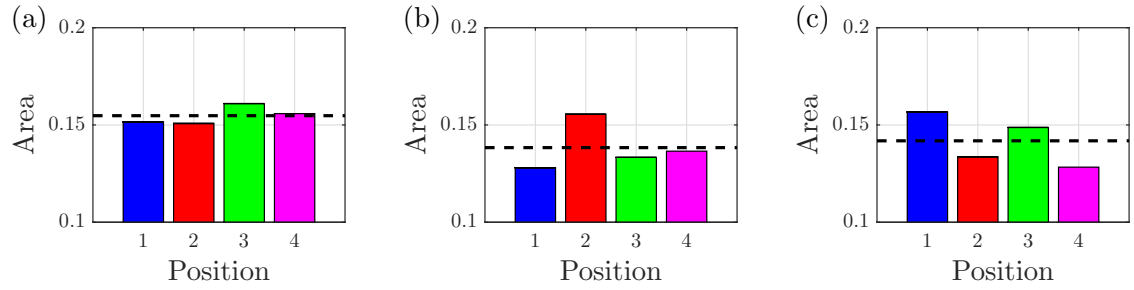

Figure 5. Areas on the intensity curves in four positions and mean for (a) N1, (b) N2 and (c) N3

The deviation between the mean curve area and the side-view areas can be performed by

$$D_{y_j} = \left| \frac{A_{y_j} - A_{y_M}}{A_{y_M}} \right| * 100\%, \tag{3}$$

where D_{y_j} is the deviation referent to j side-view, A_{y_M} is the area of mean curve and A_{y_j} is the area of the curve for the j side-view. Figure 6(a), (b) and (c) show the deviation calculated for the N1, N2 and N3 conditions, respectively.

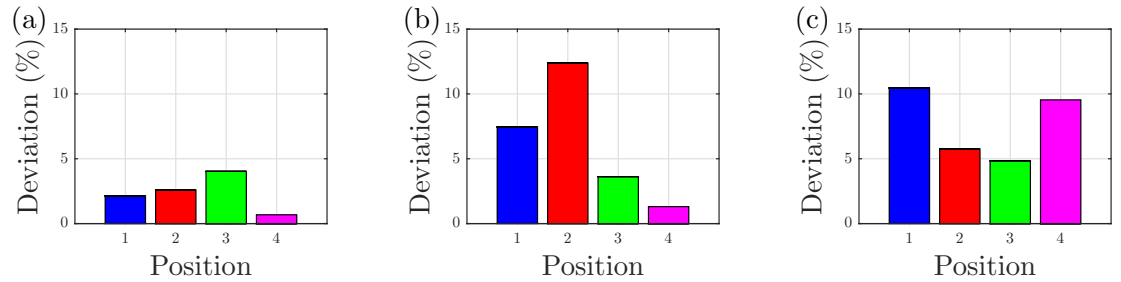

Figure 6. Deviation from area of mean signal for areas of the intensity in four positions for (a) N1, (b) N2 and (c) N3

It is observed that the deviations for the good condition nozzle is less than 5%, which is not for the N2 and N3 conditions (around 13% and 10%, respectively). This shows that such parameter can be used as an estimate of how good the health condition of spray nozzles is.

3.2 Fourier coefficients

As a method with frequency analysis, the Fourier series representation was obtained for each signal (four positions and mean). Considering the period of the signal as the normalized position interval ($T_P = 1$), the series was presented as shown by Eq. 4 adapted from Shin and Hammond (2008), in cosine terms with magnitude $C_n = \sqrt{A_n^2 + B_n^2}$, which correspond to Fourier coefficients, and phase angle $\phi_n = \arctan(-B_n/A_n)$.

$$y(x) = \frac{A_0}{2} + \sum_{n=1}^{\infty} C_n \cos(2\pi n f_1 x + \phi_n), \tag{4}$$

where x is the position, f_1 is the fundamental frequency ($f_1 = 1/T_P$), and:

$$A_0 = \frac{2}{T_P} \int_0^{T_P} y(x) dx, \tag{4a}$$

$$A_n = \frac{2}{T_P} \int_0^{T_P} y(x) \cos\left(\frac{2\pi n x}{T_P}\right) dx, \tag{4b}$$

$$B_n = \frac{2}{T_P} \int_0^{T_P} y(x) \sin\left(\frac{2\pi n x}{T_P}\right) dx. \tag{4c}$$

In computational application, the Fourier coefficients are calculated in a limited and discrete interval. Hence, 100 terms of Fourier coefficients are calculated to reconstruct the signals. Figure 7(a), (b) and (c) show the intensity vectors (PLT processed ones) in blue-solid line together with the reconstructed intensity vectors (dashed-red line) via Fourier series for the image taken in position 1 of N1, N2 and N3 conditions. It is observed that the 100 terms are enough to reconstruct the intensity vector, as they overlay very well.

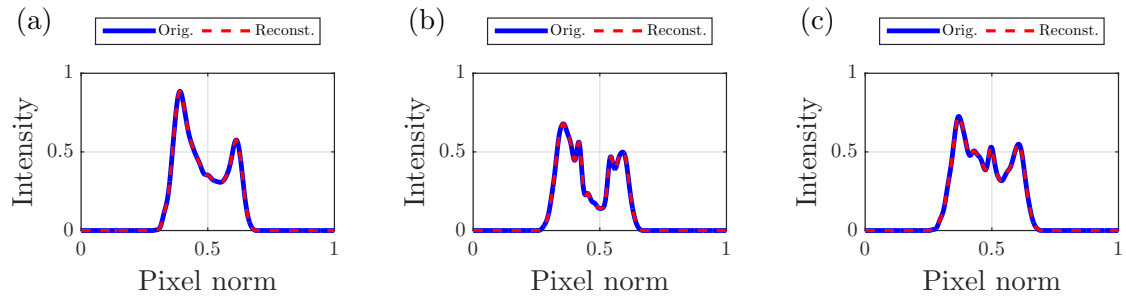

Figure 7. Intensity vectors of the PLT processed signals together with their reconstructed versions via Fourier series for (a) N1, (b) N2 and (c) N3

It is observed that the reconstructed intensity vector overlays very well to the original one, so that 100 terms are enough to calculate the Fourier coefficients. As a health condition estimation, the coefficients for the intensity signals in the four positions and for the mean signal were compared. For a good nozzle, with uniformity between side-views, is expected similar coefficients between signals, what not occur for wear nozzles. Figure 8(a), (b) and (c) show the Fourier coefficients in each frequency component for the nozzles N1, N2 and N3, respectively. Figure 8 shows the amplitude of the Fourier coefficients up 30 cycle/pixel. This is because these frequencies are the most representative of the system condition.

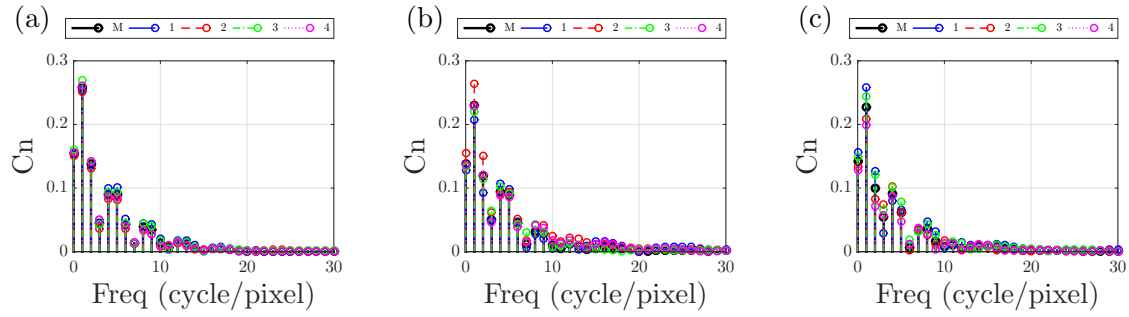

Figure 8. Fourier coefficients of calculated for the images taken at each view and their mean intensity vector signal for (a) N1, (b) N2 and (c) N3

It is observed that for lower frequencies (below 10 cycle/pixel) there is much more variability between the Fourier coefficients for the conditions N2 and N3 when compared to the condition N1. Moreover, it can be also observed that the coefficients between 10 and 20 cycle/pixel are more spreaded out within this frequency range for N2 and N3 than for N1. The N2 condition also have frequency content within 20 and 30 cycle/pixel, which cannot be clearly seem for the other

two cases. Hence, this shows that the side-view images of the N2 and N3 have different frequency content according to the position taken, which is not the case for N1 condition that has a low variability between the coefficients even between the views and the mean signal (black-solid line).

3.3 Auto-correlation

The auto-correlation function is a measure of similarity between one signal and its delay version. This tool is generally used to identify patterns present (hidden) in the data. This results in a measure of similarity as a function of the lag. Hence, the intention is to use auto-correlation function of the processed PLT intensity vectors to have another measurement of the condition of the nozzle. This can be an alternative to the Fourier coefficient to allow a straight forward visualization when compared to the mentioned tool. According to Shin and Hammond (2008) the auto-correlation can be calculated as

$$\begin{aligned} \hat{R}_{y_a}(m) &= \frac{1}{N-m} \sum_{n=0}^{N-m-1} y_a[m] y_a[n+m] && \text{para } m \geq 0, \\ &= \hat{R}_{y_a}(-m) && \text{para } m < 0. \end{aligned} \tag{5}$$

The auto-correlation has its maximum amplitude at 0 lag, which shows that the signal is equal to its delayed version (amplitude equal to one) when they are perfectly overlaid. Figure 9(a), (b) and (c) show the auto-correlation performed for each intensity vector (4 positions and mean) for the nozzles N1, N2 and N3, respectively.

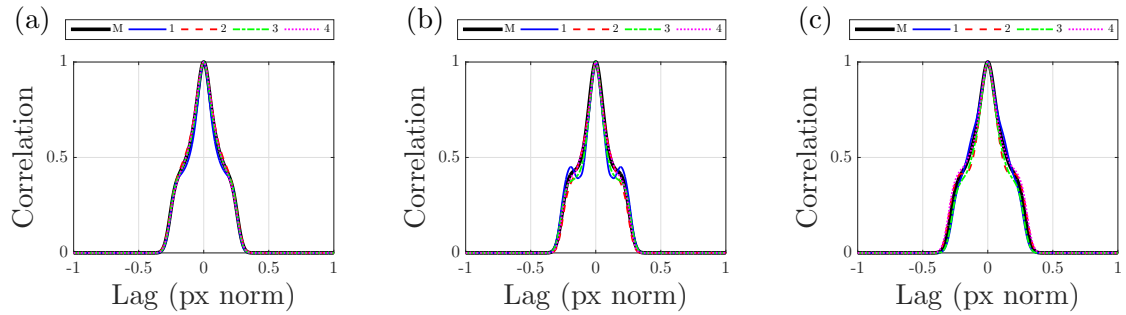

Figure 9. The auto-correlation of the intensity vectors considering the four positions and their mean for (a) N1, (b) N2 and (c) N3

It can be observed that the auto-correlation functions for the case N1 overlay really well and around the mean. This show that the images taken in any view have practically the same features. This is not the case, however, for N2 and N3. Moreover, local maximum and minimum nearby the lag 0.75 for the N2 nozzle is observed. This can be used as an indication of the nozzle condition. The angle between the x axis and a line tangent to the auto-correlation function (gradient) is calculate to give a better view how the shape of the auto-correlation changes for the N1, N2 and N3 conditions. This is shown in Fig. 10(a), (b) and (c), for the nozzles N1, N2 and N3, respectively.

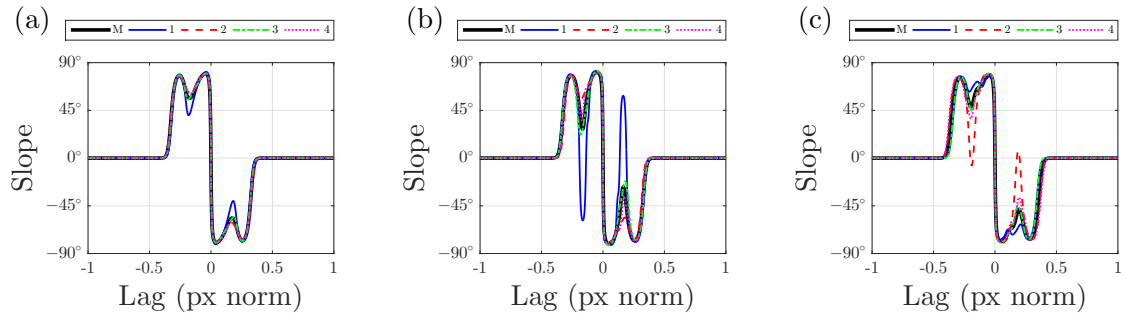

Figure 10. The slope given by a tangent line to the auto-correlation function and the x axis for the conditons (a) N1, (b) N2 and (c) N3

It is observed that the calculated slope is very similar to the nozzle in a good condition (N1), but this is not the case for N2 and N3. For these 2 nozzles there is always a peak/drop that cross the 0° line indicating the failure.

3.4 Cross-correlation

The cross-correlation is similar to the auto-correlation, however it gives a degree of similarity between two different signals, y_a and y_b. In this work these signals are the intensity vector (PLT processed ones) and the mean calculated using intensity vectors of the four images. The idea behind concerns that images from good nozzles will keep the main features independent on the position which the image is taken. Moreover, this will not differ much from the mean intensity vector. If it does, then a failure may be the cause of such change. According to Shin and Hammond (2008), the cross-correlation function can be evaluated as

$$\begin{aligned} \hat{R}_{y_a y_b}(m) &= \frac{1}{N-m} \sum_{n=0}^{N-m-1} y_a[m] y_b[n+m] && \text{para } m \geq 0, \\ &= \hat{R}_{y_b y_a}(-m) && \text{para } m < 0. \end{aligned} \tag{6}$$

The cross-correlation coefficient, which gives a normalized amplitude between 0 and 1 is used, and can be performed as

$$\hat{R}_{y_a y_b, coef}(m) = \frac{\hat{R}_{y_a y_b}(m)}{\sqrt{\hat{R}_{y_a}(0)\hat{R}_{y_b}(0)}}. \tag{7}$$

When the cross-correlation is 1, this mean that the signal is strong correlated and 0 otherwise. Figure 11(a), (b) and (c) show the cross-correlation coefficient performed between the intensity vectors (processed via PLT) and their mean for the conditions N1, N2 and N3, respectively.

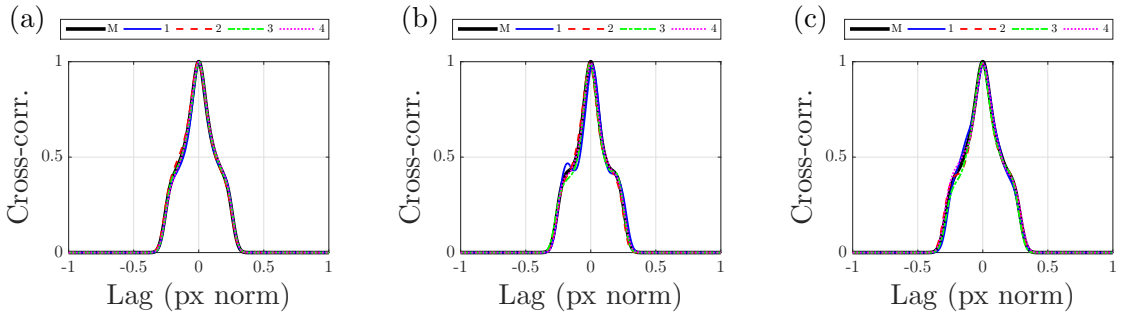

Figure 11. The cross-correlation coefficients calculated between the intensity vectors (processed via PLT) and their mean for the nozzle conditions (a) N1, (b) N2 and (c) N3

It is observed that for the N1 condition the cross-correlation functions overlay very well and around the mean, as expected. This is not the case for N2 and N3 conditions, especially for the N2 condition. The auto-correlations is clearer for these cases. Likewise for the auto-correlation, the slope is also calculated for the cross-correlation. Figure 12(a), (b) and (c), show the slope between the tangent line and the x axis for the conditions N1, N2 and N3, respectively.

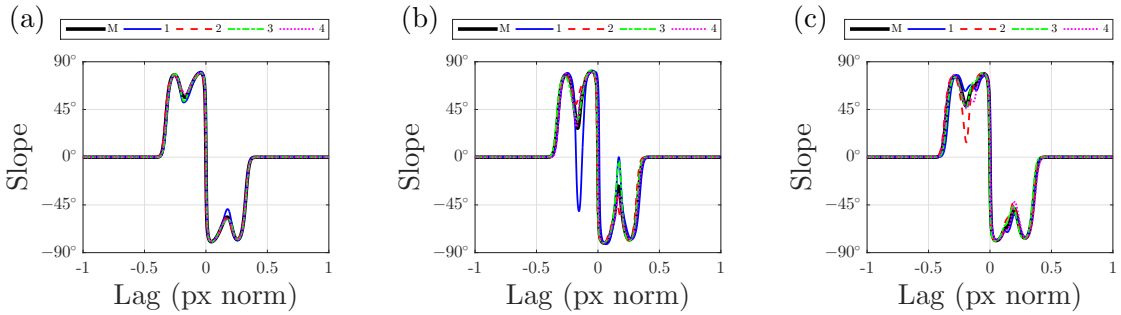

Figure 12. Slope between the tangent line to the cross-correlation function and the x axis considering the conditions (a) N1, (b) N2 and (c) N3

Likewise as observed for the auto-correlation, the slope for the cross-correlation shows peak/drop for the cases N2 and N3 as an indication of the bad health condition of such nozzles. Moreover, the degree of symmetry can also be observed, for lags below and above zero. The nozzle N1 presents a good degree of symmetry, where the slope below zero is the inverse of the slope above zero (same shapes but the other way round). This is not the case for N2 and N3.

4. CONCLUSION

The pre-processing method presented in this paper shows an effective improvement of estimating the health condition of spray nozzles. This is carried out by using the analysis of intensity levels, together with digital filters to reduce undesirable noise, and there is no need of special camera, reducing the cost of such method. The presence of wear in the nozzles can be observed in the intensity levels of the spray side-view images which are used to detect the health condition of such nozzles. Four metrics have been proposed. The area under the intensity vector, is the simplest one and gives a very good way of measuring the Nozzle condition. The Fourier Series, which gives a frequency domain analysis, shows that the failures have high frequency contents and variability between the Fourier coefficients for the cases where the nozzle is not in a good condition. The auto-correlation and cross-correlation are good tools to evaluate the similarities between the intensity vectors and their mean (this is calculated by using the four side-views). However, the auto-correlation gives a better visualization of local maximum and minimum (patterns) used to identify the fault, and the symmetry is better visualized using cross-correlation function.

5. ACKNOWLEDGEMENTS

The author would like to acknowledge CAPES (Grant # 1739988) for the financial support given to this project and to Spraying Systems Co. to support for the experimental tests.

6. REFERENCES

Barber, J., 2009. "How to pre-empt a significant profit drain: Nozzle wear". *Internal report, Spraying Systems Co.*

Bauer, F.C. and Raetano, C.G., 2004. "Perfis de distribuição volumétrica de pontas XR 11003 e TXVK-4 em diferentes condições de pulverização". *Engenharia Agrícola*, Vol. 24, pp. 364 – 373. ISSN 0100-6916.

Godinho Jr., J.D., Ruas, R.A.A., Reis, M.R., Carvalho Filho, A. and Faria, V.R., 2018. "Reduction in the spray drift of 2, 4-d in tomato using hydraulic nozzles with air induction and li-700 adjuvant". *Pesquisa Agropecuária Tropical*, Vol. 48, No. 2, pp. 134–139.

Gonzalez, R.C., Woods, R.E. and Eddins, S.L., 2008. *Digital Image Processing*. Pearson Pretice Hall, New Jersey, 3rd edition.

Kecskésné Nagy, E., Koszel, M. and Sztacho-Pekary, I., 2014. "Effect of working parameters and nozzle wear rate onto the spray quality in use of different fan flat nozzle". *Journal of Central European Agriculture*, Vol. 15, No. 1, pp. 0–0.

Krishnaswamy, M. and Krishnan, P., 2002. "Pm - power and machinery: Nozzle wear rate prediction using regression and neural network". *Biosystems Engineering*, Vol. 82, No. 1, pp. 53 – 64. ISSN 1537-5110.

Maciel, C.F.S., Teixeira, M.M., Fernandes, H.C., Zolnier, S. and Cecon, P.R., 2018. "Droplet spectrum of a spray nozzle under different weather conditions". *Revista Ciência Agronômica*, Vol. 49. ISSN 1806-6690.

Ozkan, H.E., Reichard, D.L. and Ackerman, K.D., 1992. "Effect of orifice wear on spray patterns from fan nozzles". *Transactions of the ASAE*, Vol. 35, No. 4, pp. 1091–1096.

Shin, K. and Hammond, J., 2008. *Fundamentals of signal processing for sound and vibration engineers*. John Wiley & Sons, Chichester, West Sussex.

Xu, Y. and Yan, H., 2016. "Numerical simulation of erosive wear on an impact sprinkler nozzle using a remeshing algorithm". *International Journal of Fluid Machinery and Systems*, Vol. 9, No. 4, pp. 287–299.

7. RESPONSIBILITY NOTICE

The authors are the only responsibles for the printed material included in this paper.